SUPPLEMENTARY INFORMATION

Septin 9 Exhibits Polymorphic Binding to F-actin and Inhibits Myosin and Cofilin Activity

Clayton Smith[1], Lee Dolat[2], Dimitrios Angelis[2], Eva Forgacs[1], Elias T. Spiliotis[2] and Vitold E. Galkin[1]

[1]Department of Physiological Sciences, Eastern Virginia Medical School, Norfolk, VA 23507, USA

[2]Department of Biology, Drexel University, Philadelphia, PA 19104, USA

Supplementary Figures

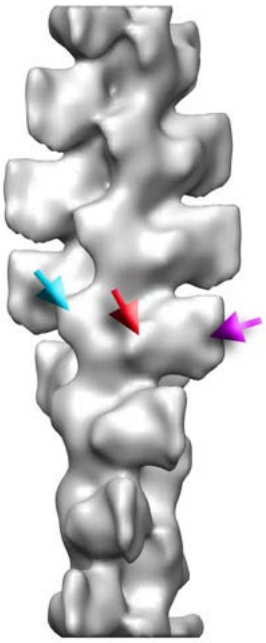

Figure S1. Overall 3D reconstruction of F-actin decorated with the NTD suggest the sites of SEPT9 binding to the actin filament. Segments of actin filaments decorated with the NTD of SEPT9 were reconstructed using IHRSR approach starting from a solid cylinder. The resultant reconstruction possessed three additional densities on the surface of F-actin. The first one is at the front interface between SD1 and SD2 of two the adjacent actin protomers (red arrow). The second density is at the side of SD1 (magenta arrow), while the third one is on the top of SD4 (cyan arrow).

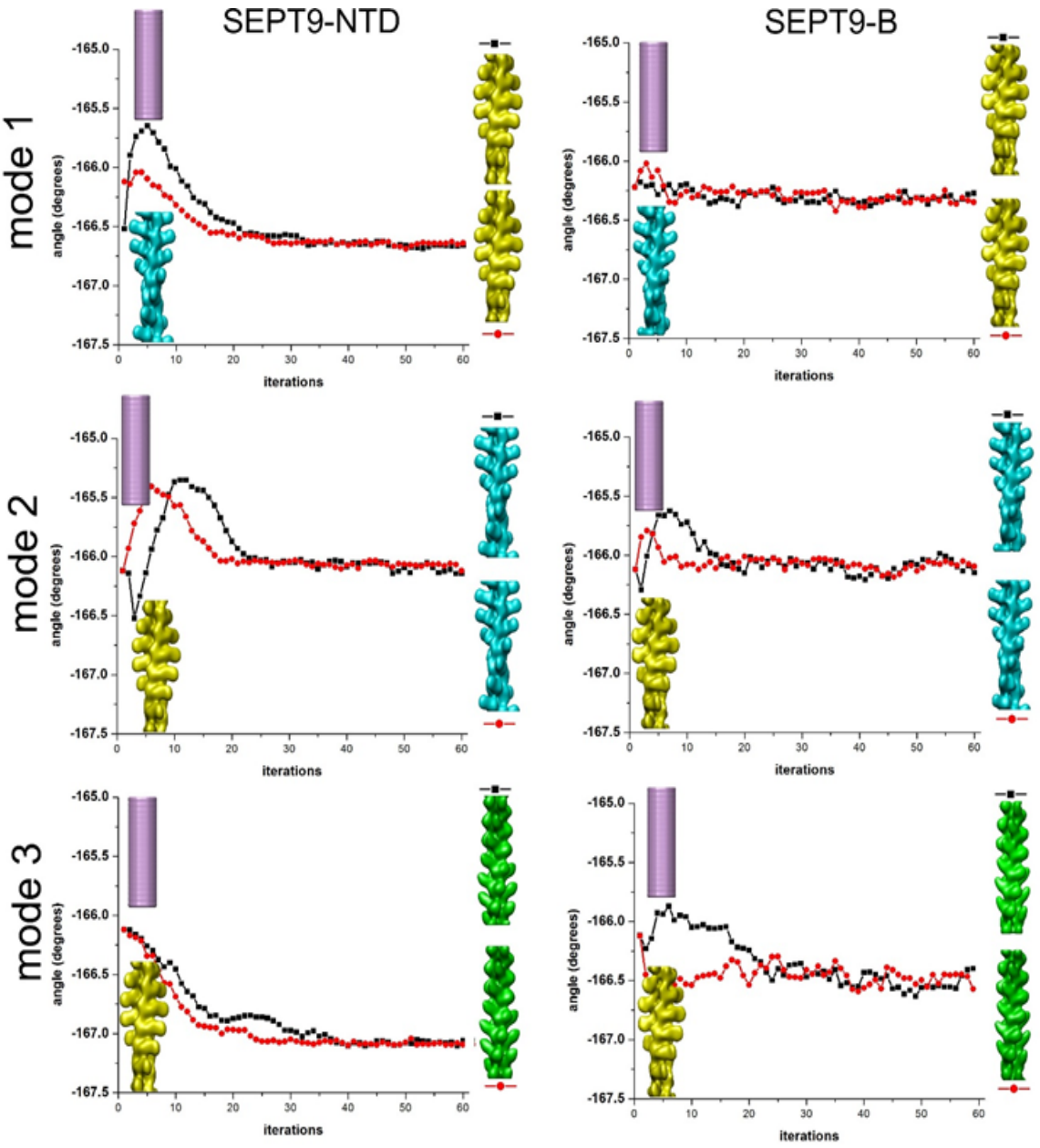

Figure S2. Convergence of structural classes validates model-based cross-correlation sorting. Every structural class was independently reconstructed using IHRSR algorithm starting from either a solid featureless cylinder (purple) or 3D reconstruction obtained from another structural class. 3D reconstructions of mode 1, mode 2 and mode 3 are shown in yellow, cyan and green, respectively. Each class converged to the same structural solution regardless of the starting model.

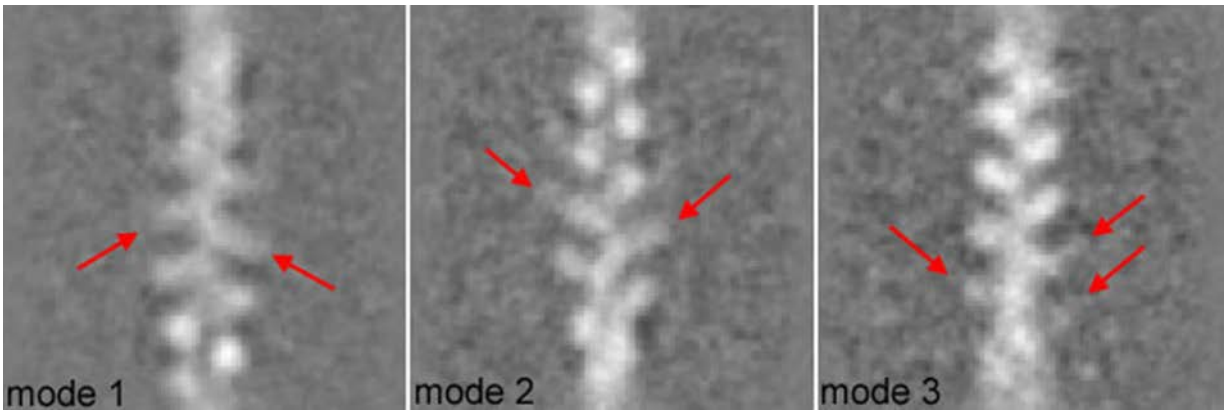

Figure S3. **Reference free 2D averages of occupied classes**. SPIDER[1] AP SR routine was used to generate reference free 2D averages of the three structural modes recovered in the NTD-decorated actin filaments. Red arrows indicate visible differences in the SEPT9-NTD positions.

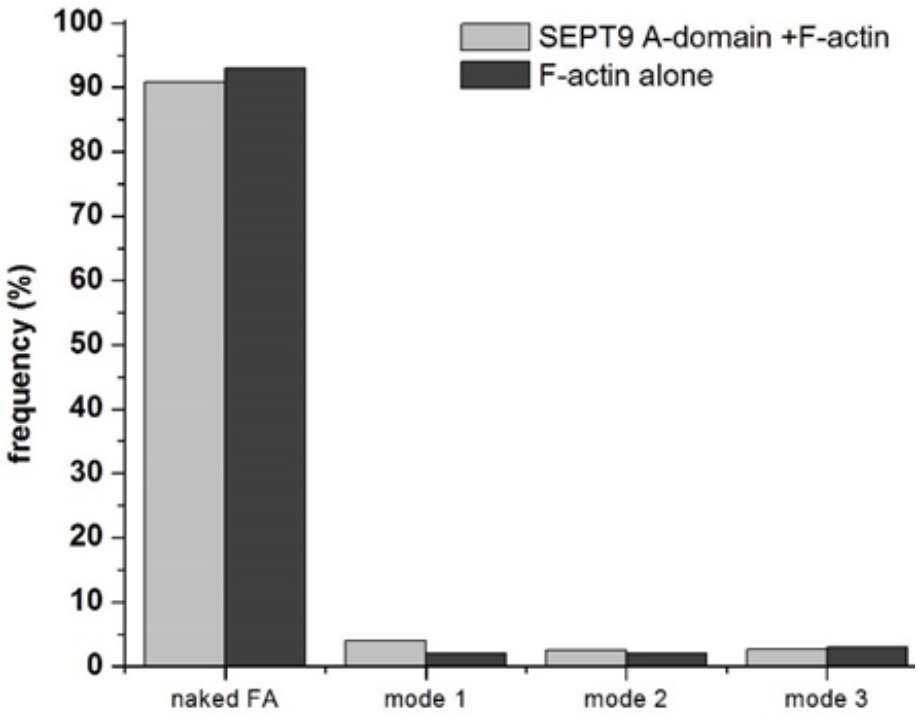

Figure S4. **Comparison of the frequencies of structural classes upon cross-correlation sorting of F-actin segments in the presence or absence of the A-domain of SEPT9**. We performed cross-correlation sorting of pure F-actin segments and F-actin segments in the presence of the A-domain using the same set of references that was employed in the sorting of the NTD-decorated F-actin segments. Comparison of the classes' frequencies does not reveal any difference between the two data sets and suggests that the small number of F-actin segments assigned to the occupied classes in the presence of A-domain is not due to the decoration by the A-domain, but rather reflects the margin of error in the sorting procedure.

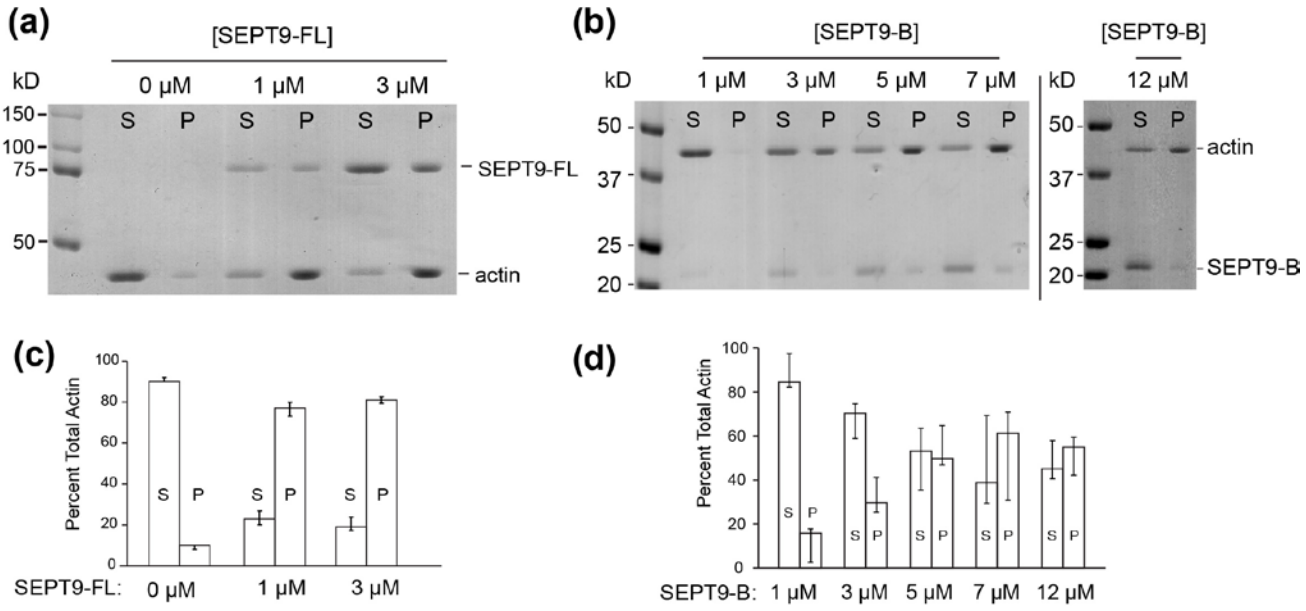

Figure S5. Full length SEPT9 and SEPT9 B-domain do not significantly affect F-actin bundling over concentration ranges that inhibit myosin activity. (a - b) Coomassie-stained SDS-PAGE gel shows the supernatant (S) and pellet (F) fractions from a low-speed actin sedimentation assays in the absence and presence of recombinant full length SEPT9 (a) or B-domain (b). (c - d) Bar graph shows the percentage of F-actin in the supernatant and pellet fractions in the absence and presence of SEPT9 (c) or B-domain (d). Error bars indicate the lowest and highest values from three independent experiments. Note that the percentage of pelleted actin is similar between 1 and 3 μM of full length SEPT9, while this concentration increase results in a 2-3-fold decrease in myosin ATPase activity (Fig. 3d). The percentage of pelleted actin is also similar in the range of 3 – 12 μM of B-domain, which causes >5-fold decrease in myosin ATPase activity (Fig. 3d).

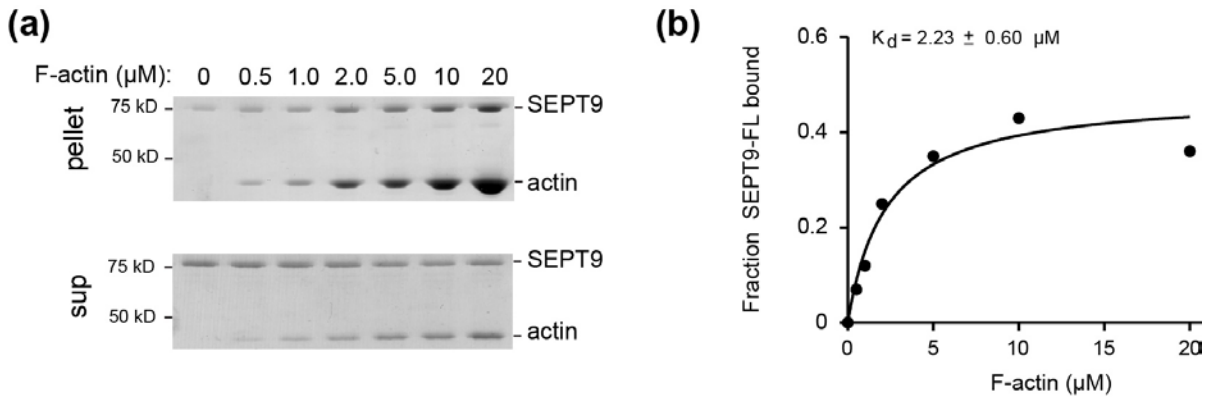

Figure S6. **Cosedimentation assay of full length SEPT9 with F-actin.** (a) Coomassie-stained gels show the pellet and supernatant fractions (equal volumes) from a representative high-speed sedimentation assay. SEPT9 (1 μM) was incubated with increasing concentrations of F-actin for 30 min at room temperature and was centrifuged at 200,000 g. (b) Binding curve shows the fraction of F-actin-bound SEPT9 as a function of increasing concentrations of F-actin. Data were fitted in GraphPad with one site specific binding curve and an estimated Kd of 2.23 ± 0.60 μM was derived based on three independent experiments.

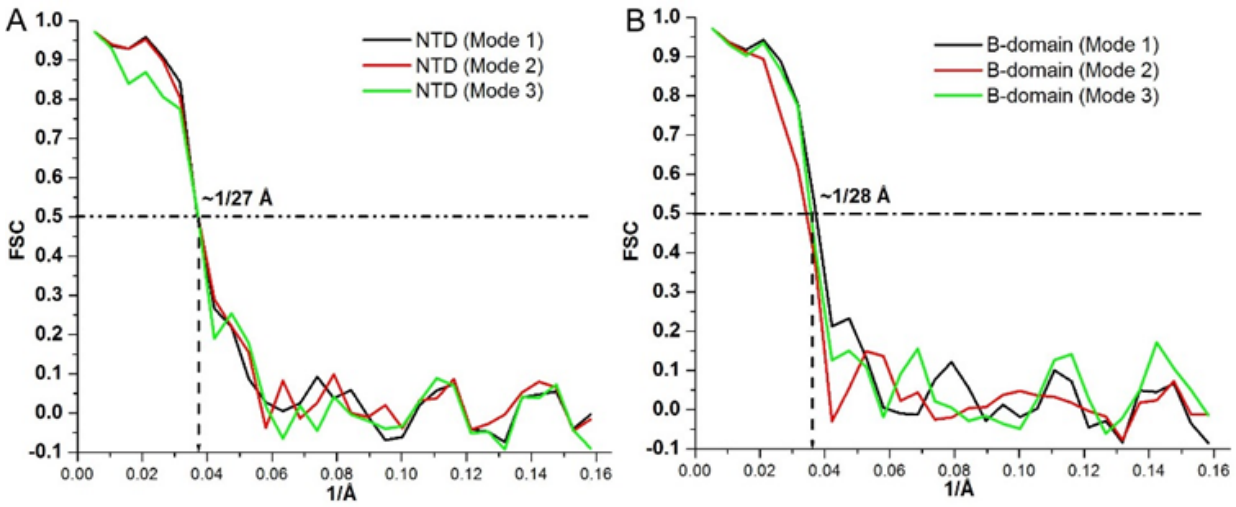

Figure S7. Resolution determination. Each structural class was split in two non-overlapping sets and the IHRSR procedure was used on each set. The correlation between the corresponding Fourier shells of the two resultant volumes was calculated for each data set.

Reference List

1. Frank, J., Shimkin, B. & Dowse, H. (1981). SPIDER - A modular software system for electron image processing. *Ultramicroscopy* **6**, 343-358.
Ref Type: Journal